Determining topological order from infinite projected entangled pair states

Anna Francuz, Jacek Dziarmaga, Guifre Vidal, and Lukasz Cincio

Determining topological order from infinite projected entangled pair states

Anna Francuz,[1] Jacek Dziarmaga,[1] Guifre Vidal,[2, 3] and Lukasz Cincio[4, *]

[1]*Institute of Physics, Jagiellonian University, Łojasiewicza 11, PL-30348 Kraków, Poland*
[2]*Perimeter Institute for Theoretical Physics, Waterloo, Ontario, N2L 2Y5 Canada*
[3]*X, The Moonshot Factory, Mountain View, CA 94043*
[4]*Theory Division, Los Alamos National Laboratory, Los Alamos, NM 87545*
(Dated: January 6, 2020)

We present a method of extracting information about the topological order from the ground state of a strongly correlated two-dimensional system computed with the infinite projected entangled pair state (iPEPS). For topologically ordered systems, the iPEPS wrapped on a torus becomes a superposition of degenerate, locally indistinguishable ground states. Projectors in the form of infinite matrix product operators (iMPO) onto states with well-defined anyon flux are used to compute topological S and T matrices (encoding mutual- and self-statistics of emergent anyons). The algorithm is shown to be robust against a perturbation driving string-net toric code across a phase transition to a ferromagnetic phase. Our approach provides accurate results near quantum phase transition, where the correlation length is prohibitively large for other numerical methods. Moreover, we used numerically optimized iPEPS describing the ground state of the Kitaev honeycomb model in the toric code phase and obtained topological data in excellent agreement with theoretical prediction.

Topologically ordered phases [1] have in recent years attracted significant attention, mostly due to the fact that they support anyonic excitations — exotic quasiparticles that obey fractional statistics. They are of interest not only from a fundamental perspective but also because of the possibility of realizing fault-tolerant quantum computation [2] based on the braiding of non-Abelian anyons. An important challenge is to identify microscopic lattice Hamiltonians that can realize such exotic phases of matter. Apart from a number of exactly solvable models [2–4], verifying whether a given microscopic Hamiltonian realizes a topologically ordered phase and accessing its properties has traditionally been regarded as an extremely hard task.

A leading computational approach is to use Density Matrix Renormalization Group (DMRG) [5, 6] on a long cylinder [7–20]. In the limit of infinitely long cylinders, DMRG naturally produces ground states with well-defined anyonic flux, from which one can obtain full characterization of a topological order, via so-called topological S and T matrices [21]. Since the proposal of Ref. [21], the study of topological order by computing the ground states of an infinite cylinder with DMRG has become a common practice [22–39].

The cost of a DMRG simulation grows exponentially with the width of cylinder, effectively restricting this approach to thin cylinders. Instead, (infinite) Projected Entangled Pair States (iPEPS) allow for much larger systems [40–42]. However, (variationally optimized) iPEPS naturally describe ground states with a superposition of anyonic fluxes. Here we show, starting with one such PEPS, how to produce a PEPS-like tensor network for each ground state with well-defined flux. Such tensor networks are suitable for extracting topological S and T matrices by computing overlaps between ground states.
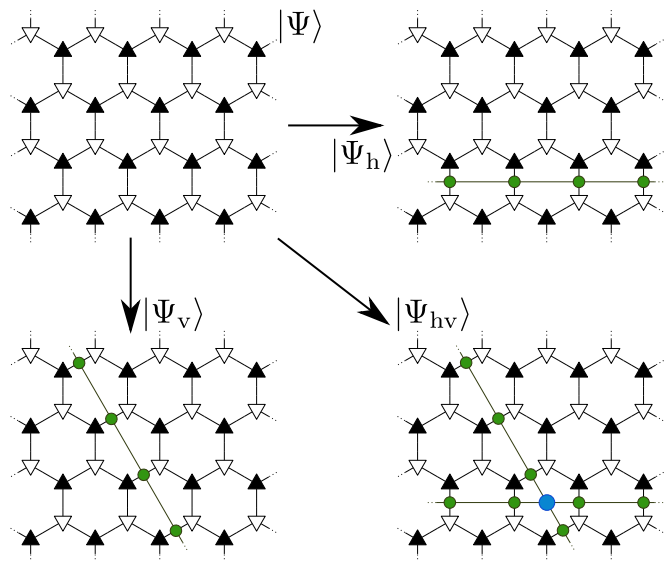
FIG. 1. A set of states $|\Psi_\mathrm{v}\rangle$, $|\Psi_\mathrm{h}\rangle$, $|\Psi_\mathrm{hv}\rangle$ is constructed from a single PEPS $|\Psi\rangle$ by inserting various MPOs in its bond indices. For a topologically ordered phase (toric code on a honeycomb lattice in this example), a proper combination of four states $|\Psi\rangle$, $|\Psi_\mathrm{v}\rangle$, $|\Psi_\mathrm{h}\rangle$ and $|\Psi_\mathrm{hv}\rangle$ is used to construct a basis of states with well-defined anyonic flux in a given direction. Physical indices are not drawn for simplicity. See text for details.

Our approach does not assume a clean realization of certain symmetries on the bond indices, in contrast to [43–46]. It also has much lower cost than methods based on the Tensor Renormalization Group [47].

In this Letter we employ variational method to minimize the energy of the iPEPS [48]. The optimized state is then wrapped on a torus and the boundary conditions (with respect to the symmetry acting on the bond indices of PEPS) are suitably modified to recover all anyonic sectors. Figure 1 presents an overview of our ap-

proach. Computations are performed in the limit of an infinitely large torus allowing for accurate description of a topologically ordered phase even for models displaying a large correlation length. For clarity, we specialize the construction to PEPS describing the toric code realized by a string-net model on a honeycomb lattice [49]. The method can be applied to other Abelian anyon models, as discussed below, and extended to non-Abelian ones [50].

In the toric code, the entanglement spectrum along the topologically nontrivial cut of a torus is supported on a vector space, which is a direct sum of four sectors, corresponding to the identity $\mathbb{I}$, bosonic e and m and fermionic ϵ fluxes:

$$\mathbb{V}^{\mathrm{TC}} = \mathbb{V}^{\mathbb{I}} \oplus \mathbb{V}^e \oplus \mathbb{V}^m \oplus \mathbb{V}^\epsilon \ . \tag{1}$$

We proceed by constructing projectors on ground states with definite anyon flux. The projectors are optimized and represented by matrix product operators (MPO). When inserted into PEPS and wrapped on the torus, the optimal MPO projects onto the desired ground state. Topological S and T matrices are extracted [51, 52] by calculating overlaps between states with well-defined flux on tori related by modular transformations.

Transfer matrices and their eigenvectors. — PEPS for a toric code on a honeycomb lattice may be characterized by two tensors A and B with elements A^i_{abc} and B^i_{abc} respectively. Here, i is a physical index and a, b, c are bond indices. Let $\mathbb{A}$ and $\mathbb{B}$ denote double tensors $\mathbb{A} = \sum_i A^i \otimes (A^i)^*$ and $\mathbb{B} = \sum_i B^i \otimes (B^i)^*$ with double bond indices $\alpha = (a, a')$, etc., see Fig. 2(A). PEPS transfer matrix (TM) Ω is defined by a line of tensors $\mathbb{A}$ and $\mathbb{B}$ contracted via some of their indices, as shown in Fig. 2(B).

For a toric code PEPS we observe that Ω contains a direct sum of $n = 2$ topological sectors. Thus, the reduced density matrix on the virtual indices (which is directly related to the physical reduced density matrix [53]) at a topologically nontrivial cut is a direct sum of two contributions

$$\mathbb{V}_{\mathrm{cut}} = \mathbb{V}^{\mathbb{I}} \oplus \mathbb{V}^e \ \Rightarrow \ \rho_{\mathrm{cut}} = \rho^{\mathbb{I}} \oplus \rho^e \ . \tag{2}$$

(recall that the ground state degeneracy of a toric code on a torus is $n^2 = 4$). The use of a pure MPS [54] as an ansatz for the dominant eigenvectors v_1, v_2 of Ω selects a specific linear combination of sectors. We note that only the method based on boundary MPS (presented here) is capable of breaking the degeneracy of the dominant eigenvectors into minimally entangled states. Methods based on corner transfer matrix treat vertical and horizontal directions on the same footing and therefore will not select a minimally entangled state in a given direction. Numerically, eigenvectors v_i may be obtained using power method or by more advanced approaches such as VUMPS algorithm [55], see Appendix A of Supplemental Material [56] for details. In the diagonal basis, they take the following form

$$v_1 = \rho^{\mathbb{I}} \oplus \rho^e \ , \quad v_2 = \rho^{\mathbb{I}} \oplus -\rho^e \ , \tag{3}$$
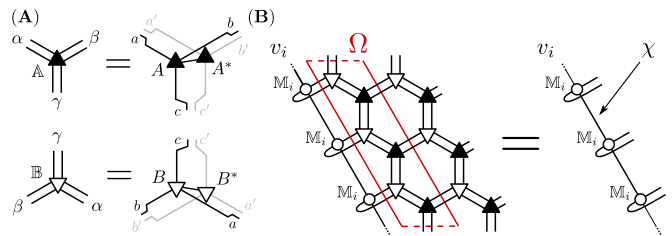
FIG. 2. (A) Graphical representation of double tensors $\mathbb{A}$ and $\mathbb{B}$. (B) Left eigenvector v_i of vertical TM Ω takes an MPO form. Vector v_i is constructed with a single tensor $\mathbb{M}_i$ with bond dimension χ, for $i = 1, 2$ and is obtained using boundary MPS method described in detail in Appendix A of Supplemental Material [56].

where we regard vector v_i as an operator represented by an MPO constructed with a single tensor $\mathbb{M}_i$ as shown in Fig. 2(B). Here, $\rho^{\mathbb{I}}$ and ρ^e are boundary density matrices in identity and bosonic sectors, respectively. For clarity, we omitted the fact that vectors v_i may contain zero component, that is $v_1 = \rho^{\mathbb{I}} \oplus \rho^e \oplus 0$ and similarly for v_2. This leads to numerical instabilities and other complications that we discuss in detail in Appendix A of Supplemental Material [56].

Matrix product description of v_1 and v_2 allows us to find an operator Z_{v} in the form of an MPO that maps v_1 into v_2 and back by demanding that

$$v_1 Z_{\mathrm{v}} = v_2 \ , \quad Z_{\mathrm{v}} v_2 = v_1 \ . \tag{4}$$

In the diagonal basis of Eq. (3), $Z_{\mathrm{v}} = \mathbb{I} \oplus -\mathbb{I}$. We stress that we are able to obtain the generator of the global $\mathbb{Z}_2$ "spin-flip" symmetry that acts on the bond indices of PEPS, even though the symmetry is not realized on-site. In other words, PEPS tensors A and B do not have to be symmetric, as required in [43–46], for our construction to work.

Similarly, we define horizontal TM Ω_{h} and obtain its $n = 2$ degenerate leading eigenvectors h_1 and h_2. Again, we are able to find an operator Z_{h} such that

$$h_1 Z_{\mathrm{h}} = h_2 \ , \quad Z_{\mathrm{h}} h_2 = h_1 \ . \tag{5}$$

Finally, we build vertical "impurity" TM $\widetilde{\Omega}_{\mathrm{v}}$ by inserting Z_{h} operator on a horizontal cut of PEPS, as shown in Fig. 3(A). Z_{h} implements anti-periodic boundary conditions with respect to $\mathbb{Z}_2$ "spin-flip" symmetry acting in the PEPS bond indices. Note that, even if the $\mathbb{Z}_2$ symmetry is not realized on site, we still know that Z_{h} changes the boundary conditions from periodic to anti-periodic. Thus, inserting Z_{h} allows us to access two remaining sectors

$$\widetilde{\mathbb{V}}_{\mathrm{cut}} = \mathbb{V}^m \oplus \mathbb{V}^\epsilon \ \Rightarrow \ \widetilde{\rho}_{\mathrm{cut}} = \rho^m \oplus \rho^\epsilon \ . \tag{6}$$

As expected, we find $n = 2$ leading eigenvectors of $\widetilde{\Omega}_{\mathrm{v}}$ that in some basis take the form

$$v_3 = \rho^m \oplus \rho^\epsilon \ , \quad v_4 = \rho^m \oplus -\rho^\epsilon \ . \tag{7}$$
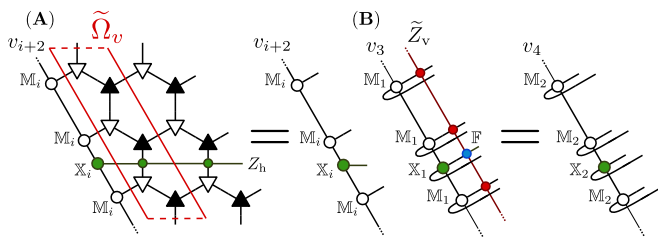
FIG. 3. (A) Two eigenvectors v_3 and v_4 are obtained as pure MPOs from v_1 and v_2 by introducing additional tensors $\mathbb{X}_1$ and $\mathbb{X}_2$, which are obtained variationally. Tensors $\mathbb{X}_i$ are chosen such that v_3 and v_4 are leading eigenvectors of "impurity" TM $\widetilde{\Omega}_{\mathrm{v}}$. Double lines are dropped to improve clarity. (B) Graphical illustration of one of the conditions for $\widetilde{Z}_{\mathrm{v}}$ in Eq. (8).

Eigenvectors v_3 and v_4 are obtained as pure MPOs [54] from v_1 and v_2 by allowing for additional tensors $\mathbb{X}_i$, as depicted in Fig. 3(A). Note that tensors $\mathbb{X}_i$ are obtained variationally. In the limit of vanishing correlation length ξ in the toric code PEPS studied here, the above ansatz for v_3 and v_4 becomes exact. In other models, bond dimension χ of all v_i is increased to account for potentially large ξ. Our ansatz is validated by the results presented below. There, the correlation length $\xi \approx 25$ does not significantly impact the quality of the final result, see Fig. 5 and the discussion below it.

$\mathbb{Z}_2$ symmetry acting on the anti-periodic sectors is realized by an operator $\widetilde{Z}_{\mathrm{v}}$ satisfying

$$v_3 \widetilde{Z}_{\mathrm{v}} = v_4 , \quad \widetilde{Z}_{\mathrm{v}} v_4 = v_3 . \tag{8}$$

The construction of $\widetilde{Z}_{\mathrm{v}}$ mirrors the one of v_3 and v_4. $\widetilde{Z}_{\mathrm{v}}$ is obtained from Z_{v} by allowing for additional variational tensor $\mathbb{F}$. Fig. 3(B) shows one condition from Eq. (8) that is used to compute $\mathbb{F}$. $\mathbb{F}$ is one of the generators of C^*-algebra, from which central idempotents can be found [44].

Appendix A of Supplemental Material [56] details some numerical issues associated with finding vectors v_i, $i = 1, \ldots, 4$ as well as solving Eqs. (4) and (8).

Projectors onto definite anyon fluxes. — Symmetry group generators Z_{v} and $\widetilde{Z}_{\mathrm{v}}$ can be used to construct ground states with well-defined flux in the horizontal direction. Recall that Z_{v} realizes $\mathbb{Z}_2$ symmetry in the periodic sector $\mathbb{V}^{\mathbb{I}} \oplus \mathbb{V}^e$. Operators $P^{\pm} = (\mathbb{I} \pm Z_{\mathrm{v}})/2$ are thus projectors on definite anyonic sectors and states

$$|\Psi^{\mathbb{I}}\rangle \sim |\Psi\rangle + |\Psi_{\mathrm{v}}\rangle , \quad |\Psi^e\rangle \sim |\Psi\rangle - |\Psi_{\mathrm{v}}\rangle \tag{9}$$

have well-defined identity and electric flux in the horizontal direction, respectively. Note that projectors $P^{\pm}$ do not act on the physical Hilbert space. Instead, they are defined on the bond indices of PEPS. The above construction is summarized in Fig. 1. Here, $|\Psi\rangle$ denotes initial PEPS state and $|\Psi_{\mathrm{v}}\rangle$ is the state obtained by inserting Z_{v} into bond indices of PEPS that defines $|\Psi\rangle$. We
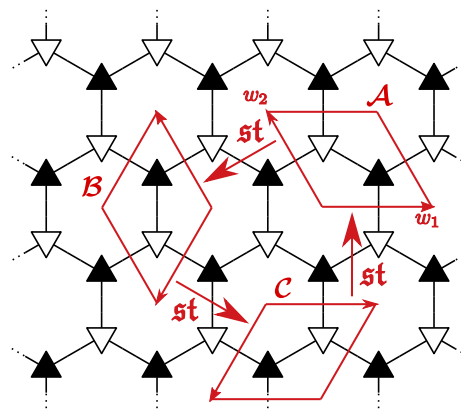
FIG. 4. Three tori $\mathcal{A}$, $\mathcal{B}$ and $\mathcal{C}$ on a honeycomb lattice considered in our method. Torus $\mathcal{A}$ is defined by a pair of vectors (w_1, w_2). Each torus is obtained by $\mathfrak{st}$ modular transformation from another torus. Transformation $\mathfrak{st}$ corresponds to $120°$ rotation, $(\mathfrak{st})^3 = \mathbb{I}$. The described approach requires $120°$ rotation symmetry of the lattice. Generalization to other symmetries is straightforward. Physical indices are not drawn for simplicity.

remark that projectors $P^{\pm}$ play the same role as projector MPO's in construction of MPO-injective PEPS [44].

Similarly, $\widetilde{Z}_{\mathrm{v}}$ generates $\mathbb{Z}_2$ symmetry group in the anti-periodic sector $\mathbb{V}^m \oplus \mathbb{V}^\epsilon$. It defines projectors $\widetilde{P}^{\pm} = (\mathbb{I} \pm \widetilde{Z}_{\mathrm{v}})/2$. States with well-defined magnetic $|\Psi^m\rangle$ and fermionic $|\Psi^\epsilon\rangle$ flux are obtained by first changing the boundary conditions on the bond indices with Z_{h} and then projecting onto the proper subspace. That is,

$$|\Psi^m\rangle \sim |\Psi_{\mathrm{h}}\rangle + |\Psi_{\mathrm{hv}}\rangle , \quad |\Psi^\epsilon\rangle \sim |\Psi_{\mathrm{h}}\rangle - |\Psi_{\mathrm{hv}}\rangle , \tag{10}$$

where $|\Psi_{\mathrm{h}}\rangle$ stands for $|\Psi\rangle$ with Z_{h} inserted and $|\Psi_{\mathrm{hv}}\rangle$ denotes $|\Psi_{\mathrm{h}}\rangle$ that has $\widetilde{Z}_{\mathrm{v}}$ embedded in together with the tensor $\mathbb{F}$. Figure 1 summarizes the construction of $|\Psi_{\mathrm{h}}\rangle$ and $|\Psi_{\mathrm{hv}}\rangle$.

Topological S and T matrices. — States $|\Psi^i\rangle$ with well-defined flux $i = \mathbb{I}, e, m, \epsilon$ are used to calculate topological S and T matrices. T matrix is diagonal and stands for self-statistics, while S matrix encodes mutual statistics. Together they form a representation of a modular group $SL(2, \mathbb{Z})$, by which they are related to the modular transformations of a torus generated by $\mathfrak{s}$ and $\mathfrak{t}$ transformations [57]. It follows that overlaps between $|\Psi^i\rangle$ transformed by a combination of modular transformations $\mathfrak{s}$ and $\mathfrak{t}$ constitute entries of a corresponding combination of topological S and T matrices.

Throughout this paper, for concreteness, we work with the transformations on a lattice with $120°$ rotational symmetry. The construction is however general and applicable to lattices with other symmetries as well. We start by defining torus $\mathcal{A}$ in Fig. 4 with unit vectors w_1, w_2 and corresponding transfer matrices: vertical $(w_1, N_v w_2)$ and horizontal $(N_h w_1, w_2)$, see Fig. 2(B) for comparison. Similarly, we consider tori $\mathcal{B}$ and $\mathcal{C}$ together with their corresponding transfer matrices as shown in Fig. 4.
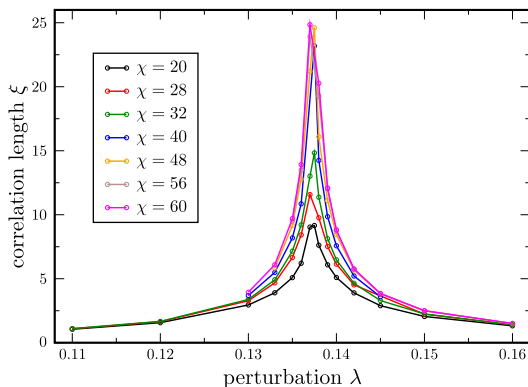
FIG. 5. Correlation length ξ as a function of perturbation strength λ and a bond dimension χ of the TM eigenvectors v_i. Increasing χ reveals a quantum phase transition at $\lambda = 0.137...0.138$. It separates toric code and ferromagnetic phases.

FIG. 6. Correlation length ξ as a function of $J_x = J_y$ in the Kitaev honeycomb model. Results for several values of bond dimension χ of TM eigenvectors v_i are shown. Inset: graphical illustration of Hamiltonian defined in Eq. (13) displaying three different types of coupling: x, y and z.

Our method requires finding three complete sets of ground states

$$\left\{|\Psi_{\mathcal{A}}^i\rangle\right\}, \quad \left\{|\Psi_{\mathcal{B}}^i\rangle\right\}, \quad \left\{|\Psi_{\mathcal{C}}^i\rangle\right\}, \quad i = \mathbb{I}, e, m, \epsilon \quad (11)$$

with well-defined anyon fluxes corresponding to three different tori: $\mathcal{A}$, $\mathcal{B}$, $\mathcal{C}$. Each torus is related to the previous one by a modular transformation $\mathfrak{st}$, which generates $120°$ counterclockwise rotation, see Fig. 4. Topological S and T matrices are extracted from all possible overlaps between states in (11). This computation is presented in [52] and described in Appendix B of Supplemental Material [56]. We stress that presented method does not require any rotational invariance of the iPEPS tensors.

Toric code versus double semion and quantum double of $\mathbb{Z}_3$. — PEPS tensors that represent ground states of string-net models on a honeycomb lattice with zero correlation length can be found analytically [4, 58]. As a proof of principle, we numerically obtain topological S and T matrices for the toric code and the double semion model. Moreover, the described method gave exact S and T matrices for the quantum double of $\mathbb{Z}_3$ model defined on a square lattice [59]. In this Letter we restrict the description to the toric code phase realized in (i) perturbed string-net model and (ii) Kitaev honeycomb model for which we analyze iPEPS ground state obtained by numerical energy optimization.

Perturbed string-net model. — In order to drive the iPEPS away from the fixed point with zero correlation length, we apply a perturbation $e^{-\lambda V}$ towards a ferromagnetic phase similarly as in [60–62] but with a two-site interaction $V = -\sum_{\langle i,j\rangle} \sigma_i^x \sigma_j^x$, see Appendix C of Supplemental Material [56].

Our method allows us to obtain accurate results even close to the critical point, in the regime of very long correlation lengths ξ, see Fig. 5. Indeed, for $\lambda = 0.136$, where $\xi \approx 25$, we obtain $S = S_{\text{tc}} + \epsilon_S$, $T = T_{\text{tc}} + \epsilon_T$,

where:

$$S_{\text{tc}} = \frac{1}{2}\begin{pmatrix} 1 & 1 & 1 & 1 \\ 1 & 1 & -1 & -1 \\ 1 & -1 & 1 & -1 \\ 1 & -1 & -1 & 1 \end{pmatrix}, \qquad T_{\text{tc}} = \begin{pmatrix} 1 & 0 & 0 & 0 \\ 0 & 1 & 0 & 0 \\ 0 & 0 & 1 & 0 \\ 0 & 0 & 0 & -1 \end{pmatrix}. \quad (12)$$

The maximal element of $|\epsilon_S|$ and $|\epsilon_T|$ is of the order of 10^{-3} and 10^{-8}, respectively.

In the ferromagnetic phase we find two eigenvectors of TM Ω, $v_1 = \rho_1 \oplus 0$ and $v_2 = 0 \oplus \rho_2$. However, in contrast to topologically ordered phase described by Eq. (4), there is no operator that maps v_1 to v_2. Numerically, this situation is detected by monitoring the distance (per lattice site) between $v_1 Z_v$ and v_2. In topologically trivial phase the distance converges to a finite value with growing bond dimension of v_i.

Kitaev honeycomb model. — The model is defined by the following Hamiltonian

$$\mathcal{H} = -\sum_{\alpha=x,y,z} J_\alpha \sum_{\alpha \text{ links}} \sigma_i^\alpha \sigma_j^\alpha \quad (13)$$

on a honeycomb lattice. Here, σ_i^α, $\alpha = x, y, z$ are Pauli matrices acting on site i. We set $J_z = 1$ and study the model along the line $J_x = J_y \in (0, 0.5)$, see Fig. 6. The iPEPS ground state is obtained using variational optimization. We find that the bond dimension $\chi = 4$ of boundary MPO's v_i suffices to faithfully capture the entanglement properties of the phase.

We obtain correct topological S and T matrices within very small error. We are able to uniquely determine the anyon model for a range of parameters $J_x = J_y \in [0.2, 0.48]$. Most notably for $J_x = J_y = 0.44$, which is close to the critical point at $J_x = J_y = 0.5$, we compute topological matrices $S = S_{\text{tc}} + \epsilon_S$, $T = T_{\text{tc}} + \epsilon_T$, where the maximal element of $|\epsilon_S|$ ($|\epsilon_T|$) is $1.3 \cdot 10^{-3}$ ($2.2 \cdot 10^{-3}$). The errors $|\epsilon_S|$, $|\epsilon_T|$ grow with increasing J, however stay below 4% in the interval $J_x = J_y \in [0.2, 0.48]$. This accuracy is sufficient to unambiguously determine the type of topological order.

Conclusions. — We presented a method of identifying topological order from microscopic lattice Hamiltonian that does not have explicit limitations on the size of the system. The method is based on extracting topological S and T matrices from a single iPEPS. Our techniques allow us to analyze systems with much bigger correlation length than the state-of-the-art 2D DMRG. Finally, we analyzed numerically optimized iPEPS describing ground state of Kitaev honeycomb model in the toric code phase. This computation shows that our approach does not require an artificially implemented realization of topological symmetries. Instead, it is applicable to generic, variationally obtained iPEPS.

[1] X. G. Wen, "Topological Orders in Rigid States," Int. J. Mod. Phys. B **4**, 239–271 (1990).

[2] A. Kitaev, "Fault-tolerant quantum computation by anyons," Annals of Physics **303**, 2–30 (2003).

[3] A. Kitaev, "Anyons in an exactly solved model and beyond," Annals of Physics **321**, 2–111 (2006).

[4] M. A. Levin and X.-G. Wen, "String-net condensation: A physical mechanism for topological phases," Phys. Rev. B **71**, 045110 (2005).

[5] S. R. White, "Density matrix formulation for quantum renormalization groups," Phys. Rev. Lett. **69**, 2863 (1992).

[6] S. R. White, "Density-matrix algorithms for quantum renormalization groups," Phys. Rev. B **48**, 10345 (1993).

[7] S. Yan, D. A. Huse, and S. R. White, "Spin-Liquid Ground State of the $S = 1/2$ Kagome Heisenberg Antiferromagnet," Science **332**, 1173 (2011).

[8] H.-C. Jiang, Z. Wang, and L. Balents, "Identifying topological order by entanglement entropy," Nature Physics **8**, 902–905 (2012).

[9] S.-S. Gong, D. N. Sheng, O. I. Motrunich, and M. P. A. Fisher, "Phase diagram of the spin-1/2 $J_1 - J_2$ Heisenberg model on a honeycomb lattice," Phys. Rev. B **88**, 165138 (2013).

[10] Z. Zhu, D. A. Huse, and S. R. White, "Weak Plaquette Valence Bond Order in the $S = 1/2$ Honeycomb $J_1 - J_2$ Heisenberg Model," Phys. Rev. Lett. **110**, 127205 (2013).

[11] S.-S. Gong, W. Zhu, and D. N. Sheng, "Emergent Chiral Spin Liquid: Fractional Quantum Hall Effect in a Kagome Heisenberg Model," Scientific Reports **4**, 6317 (2014).

[12] Z. Zhu and S. R. White, "Quantum phases of the frustrated XY models on the honeycomb lattice," Modern Physics Letters B **28**, 1430016 (2014).

[13] S.-S. Gong, W. Zhu, L. Balents, and D. N. Sheng, "Global phase diagram of competing ordered and quantum spin-liquid phases on the kagome lattice," Phys. Rev. B **91**, 075112 (2015).

[14] W.-J. Hu, S.-S. Gong, W. Zhu, and D. N. Sheng, "Competing spin-liquid states in the spin-1/2 Heisenberg model on the triangular lattice," Phys. Rev. B **92**, 140403 (2015).

[15] W. Zhu, S. S. Gong, D. N. Sheng, and L. Sheng, "Possible non-Abelian Moore-Read state in double-layer bosonic fractional quantum Hall system," Phys. Rev. B **91**, 245126 (2015).

[16] Z. Zhu and S. R. White, "Spin liquid phase of the $S = 1/2$ $J_1 - J_2$ Heisenberg model on the triangular lattice," Phys. Rev. B **92**, 041105 (2015).

[17] M. P. Zaletel, Z. Zhu, Y.-M. Lu, A. Vishwanath, and S. R. White, "Space Group Symmetry Fractionalization in a Chiral Kagome Heisenberg Antiferromagnet," Phys. Rev. Lett. **116**, 197203 (2016).

[18] T.-S. Zeng, W. Zhu, J.-X. Zhu, and D. N. Sheng, "Nature of continuous phase transitions in interacting topological insulators," Phys. Rev. B **96**, 195118 (2017).

[19] M.-S. Vaezi and A. Vaezi, "Numerical Observation of Parafermion Zero Modes and their Stability in 2D Topological States," (2017), arXiv:1706.01192 [quant-ph].

[20] Z. Zhu, I. Kimchi, D. N. Sheng, and L. Fu, "Robust non-Abelian spin liquid and a possible intermediate phase in the antiferromagnetic Kitaev model with magnetic field," Phys. Rev. B **97**, 241110 (2018).

[21] L. Cincio and G. Vidal, "Characterizing Topological Order by Studying the Ground States on an Infinite Cylinder," Phys. Rev. Lett. **110**, 067208 (2013).

[22] Y.-C. He, D. N. Sheng, and Y. Chen, "Chiral Spin Liquid in a Frustrated Anisotropic Kagome Heisenberg Model," Phys. Rev. Lett. **112**, 137202 (2014).

[23] W. Zhu, S. S. Gong, F. D. M. Haldane, and D. N. Sheng, "Topological characterization of the non-Abelian Moore-Read state using density-matrix renormalization group," Phys. Rev. B **92**, 165106 (2015).

[24] W. Zhu, S. S. Gong, and D. N. Sheng, "Chiral and critical spin liquids in a spin-1/2 kagome antiferromagnet," Phys. Rev. B **92**, 014424 (2015).

[25] B. Bauer, L. Cincio, B. P. Keller, M. Dolfi, G. Vidal, S. Trebst, and A. W. W. Ludwig, "Chiral spin liquid and emergent anyons in a Kagome lattice Mott insulator," Nat. Commun. **5**, 5137 (2014).

[26] W. Zhu, S. S. Gong, F. D. M. Haldane, and D. N. Sheng, "Fractional Quantum Hall States at $\nu = 13/5$ and $12/5$ and Their Non-Abelian Nature," Phys. Rev. Lett. **115**, 126805 (2015).

[27] A. G. Grushin, J. Motruk, M. P. Zaletel, and F. Pollmann, "Characterization and stability of a fermionic $\nu = 1/3$ fractional Chern insulator," Phys. Rev. B **91**, 035136 (2015).

[28] Y.-C. He, S. Bhattacharjee, F. Pollmann, and R. Moessner, "Kagome chiral spin liquid as a gauged $U(1)$ symmetry protected topological phase," Phys. Rev. Lett. **115**, 267209 (2015).

[29] Y.-C. He and Y. Chen, "Distinct Spin Liquids and Their Transitions in Spin-1/2 XXZ Kagome Antiferromagnets," Phys. Rev. Lett. **114**, 037201 (2015).

[30] Y.-C. He, S. Bhattacharjee, R. Moessner, and F. Pollmann, "Bosonic integer quantum hall effect in an interacting lattice model," Phys. Rev. Lett. **115**, 116803 (2015).

[31] S. Geraedts, M. P. Zaletel, Z. Papić, and R. S. K. Mong, "Competing Abelian and non-Abelian topological orders in $\nu = 1/3 + 1/3$ quantum Hall bilayers," Phys. Rev. B **91**, 205139 (2015).

[32] R. S. K. Mong, M. P. Zaletel, F. Pollmann, and Z. Papić, "Fibonacci anyons and charge density order in the 12/5 and 13/5 quantum Hall plateaus," Phys. Rev. B **95**, 115136 (2017).

[33] Y.-C. He, F. Grusdt, A. Kaufman, M. Greiner, and A. Vishwanath, "Realizing and adiabatically preparing bosonic integer and fractional quantum Hall states in optical lattices," Phys. Rev. B **96**, 201103 (2017).

[34] E. M. Stoudenmire, D. J. Clarke, R. S. K. Mong, and J. Alicea, "Assembling Fibonacci Anyons From a Z_3 Parafermion Lattice Model," Phys. Rev. B **91**, 235112 (2015).

[35] Y.-C. He, M. P. Zaletel, M. Oshikawa, and F. Pollmann, "Signatures of Dirac cones in a DMRG study of the Kagome Heisenberg model," Phys. Rev. X **7**, 031020 (2017).

[36] S. N. Saadatmand and I. P. McCulloch, "Symmetry fractionalization in the topological phase of the spin-1/2 $J_1 - J_2$ triangular Heisenberg model," Phys. Rev. B **94**, 121111 (2016).

[37] C. Hickey, L. Cincio, Z. Papić, and A. Paramekanti, "Haldane-Hubbard Mott Insulator: From Tetrahedral Spin Crystal to Chiral Spin Liquid," Phys. Rev. Lett. **116**, 137202 (2016).

[38] M. P. Zaletel, Y.-M. Lu, and A. Vishwanath, "Measuring space-group symmetry fractionalization in Z_2 spin liquids," Phys. Rev. B **96**, 195164 (2017).

[39] T.-S. Zeng, W. Zhu, and D. Sheng, "Tuning topological phase and quantum anomalous Hall effect by interaction in quadratic band touching systems," npj Quantum Materials **3**, 49 (2018).

[40] F. Verstraete and J. I. Cirac, "Renormalization algorithms for Quantum-Many Body Systems in two and higher dimensions," (2004), arXiv:cond-mat/0407066.

[41] V. Murg, F. Verstraete, and J. I. Cirac, "Variational study of hard-core bosons in a two-dimensional optical lattice using projected entangled pair states," Phys. Rev. A **75**, 033605 (2007).

[42] F. Verstraete, V. Murg, and J. I. Cirac, "Matrix product states, projected entangled pair states, and variational renormalization group methods for quantum spin systems," Advances in Physics **57**, 143–224 (2008).

[43] M. B. Şahinoğlu, D. Williamson, N. Bultinck, M. Mariën, J. Haegeman, N. Schuch, and F. Verstraete, "Characterizing Topological Order with Matrix Product Operators," (2014), arXiv:1409.2150 [quant-ph].

[44] N. Bultinck, M. Mariën, D. J. Williamson, M. B. Şahinoğlu, J. Haegeman, and F. Verstraete, "Anyons and matrix product operator algebras," Annals of Physics **378**, 183–233 (2017).

[45] M. Iqbal, K. Duivenvoorden, and N. Schuch, "Study of anyon condensation and topological phase transitions from a Z_4 topological phase using the projected entangled pair states approach," Phys. Rev. B **97**, 195124 (2018).

[46] C. Fernández-González, R. S. K. Mong, O. Landon-Cardinal, D. Pérez-García, and N. Schuch, "Constructing topological models by symmetrization: A projected entangled pair states study," Phys. Rev. B **94**, 155106 (2016).

[47] H. He, H. Moradi, and X.-G. Wen, "Modular matrices as topological order parameter by a gauge-symmetry-preserved tensor renormalization approach," Phys. Rev. B **90**, 205114 (2014).

[48] P. Corboz, "Variational optimization with infinite projected entangled-pair states," Phys. Rev. B **94**, 035133 (2016).

[49] M. A. Levin and X.-G. Wen, "String-net condensation: A physical mechanism for topological phases," Phys. Rev. B **71**, 045110 (2005).

[50] A. Francuz *et al.*, *in preparation*.

[51] Y. Zhang, T. Grover, A. Turner, M. Oshikawa, and A. Vishwanath, "Quasiparticle statistics and braiding from ground-state entanglement," Phys. Rev. B **85**, 235151 (2012).

[52] Y. Zhang, T. Grover, and A. Vishwanath, "General procedure for determining braiding and statistics of anyons using entanglement interferometry," Phys. Rev. B **91**, 035127 (2015).

[53] J. I. Cirac, D. Poilblanc, N. Schuch, and F. Verstraete, "Entanglement spectrum and boundary theories with projected entangled-pair states," Phys. Rev. B **83**, 245134 (2011).

[54] The notions of pure MPSs and pure MPOs are introduced in Appendix A of Supplemental Material [56].

[55] L. Vanderstraeten, J. Haegeman, and F. Verstraete, "Tangent-space methods for uniform matrix product states," SciPost Phys. Lect. Notes , 7 (2019).

[56] See Supplemental Material at [URL] for details on numerical methods used in the main text that were omitted for clarity.

[57] X.-G. Wen, "A theory of 2+1d bosonic topological orders," National Science Review **3**, 68–106 (2015).

[58] O. Buerschaper, M. Aguado, and G. Vidal, "Explicit tensor network representation for the ground states of string-net models," Phys. Rev. B **79**, 085119 (2009).

[59] M. D. Schulz, S. Dusuel, R. Orus, J. Vidal, and K. P. Schmidt, "Breakdown of a perturbed topological phase," New Journal of Physics **14**, 025005 (2012).

[60] J. Haegeman, K. Van Acoleyen, N. Schuch, J. I. Cirac, and F. Verstraete, "Gauging quantum states: From global to local symmetries in many-body systems," Phys. Rev. X **5**, 011024 (2015).

[61] J. Haegeman, V. Zauner, N. Schuch, and F. Verstraete, "Shadows of anyons and the entanglement structure of topological phases," Nature Communications **6**, 8284

(2015).

[62] G.-Y. Zhu and G.-M. Zhang, "Gapless coulomb state emerging from a self-dual topological tensor-network state," Phys. Rev. Lett. **122**, 176401 (2019).

[63] R. N. C. Pfeifer, G. Evenbly, S. Singh, and G. Vidal, "Ncon: A tensor network contractor for matlab," (2014), arXiv:1402.0939 [physics.comp-ph].

[64] I. P. McCulloch, "Infinite size density matrix renormalization group, revisited," (2008), arXiv:0804.2509 [cond-mat.str-el].

[65] J. Jordan, R. Orús, G. Vidal, F. Verstraete, and J. I. Cirac, "Classical simulation of infinite-size quantum lattice systems in two spatial dimensions," Phys. Rev. Lett. **101**, 250602 (2008).

[66] H. N. Phien, J. A. Bengua, H. D. Tuan, P. Corboz, and R. Orús, "Infinite projected entangled pair states algorithm improved: Fast full update and gauge fixing," Phys. Rev. B **92**, 035142 (2015).